Inhibitory Mode of 1,5-Diarylpyrazole Derivatives against Cyclooxygenase-2 and Cyclooxygenase-1: Molecular Docking and 3D QSAR Analyses

Hong Liu, Xiaoqin Huang, Jianhua Shen,* Xiaomin Luo, Minghui Li, Bing Xiong, Gang Chen, Jingkang Shen, Yimin Yang, Hualiang Jiang,* and Kaixian Chen

Center for Drug Discovery and Design, State Key Laboratory of Drug Research, Shanghai Institute of Materia Medica, Shanghai Institutes for Biological Sciences, Chinese Academy of Sciences, 294 Taiyuan Road, Shanghai 200031, People's Republic of China

The Lamarckian genetic algorithm of AutoDock 3.0 has been employed to dock 40 1,5-diarylpyrazole class compounds into the active sites of cyclooxygenase-2 (COX-2) and cyclooxygenase-1 (COX-1). The binding models were demonstrated in the aspects of inhibitor's conformation, subsite interaction, and hydrogen bonding. The data of geometrical parameters and RMSD values compared with the known inhibitor, SC-558 (43), show that these inhibitors interact respectively with COX-2 and COX-1 in a very similar way. The r^2 values of 0.648 for COX-2 and 0.752 for COX-1 indicate that the calculated binding free energies correlate well with the inhibitory activities. The structural and energetic differences in inhibitory potencies of 1,5-diarylpyrazoles were reasonably explored, and the COX-2/COX-1 selectivity was demonstrated by the three-dimensional (3D) interaction models of inhibitors complexing with these two enzymes. Using the binding conformations of 1,5-diarylpyrazoles, consistent and highly predictive 3D quantitative structure–activity relationship (QSAR) models were developed by performing comparative molecular field analyses (CoMFA) and comparative molecular similarity analyses (CoMSIA). The q^2 values are 0.635 and 0.641 for CoMFA and CoMSIA models, respectively. The predictive ability of these models was validated by SC-558 (**43**) and a set of 10 other compounds that were not included in the training set. Mapping these models back to the topology of the active site of COX-2 leads to a better understanding of vital diarylpyrazole compounds and COX-2 interactions. Structure-based investigations and the final 3D QSAR results provided possible guidelines and accurate activity predictions for novel inhibitor design.

Introduction

Nonsteroidal antiinflammatory drugs (NSAIDs) display their antiinflammatory action mainly through inhibition of cyclooxygenase (COX), the key enzyme associated with arachidonic acid (AA) metabolism.[1–3] The classical NSAIDs act via inhibition of the enzyme prostaglandin (PG) H₂ synthase also referred to as COX.[1–3] This enzyme bis-oxygenates AA to PGs G₂ (PGG₂), which is subsequently degraded to vasoactive and inflammatory mediators such as PGs, prostacyclin (PGI₂), and tromboxane A₂.[4–7] Beyond their therapeutic utility, traditional NSAIDs possess predictable side effects including dyspepsia, gastrointestinal (GI) ulceration, and antiplatelet activity. It is now well-established that COX has two isoforms, i.e., COX-1 and COX-2.[4–7] COX-1 is responsible for production of basal levels of PGs needed for GI tract homeostasis, proper renal filtration rate, and platelet aggregatory function.[4–7] Biosynthesis of the COX-2 enzyme is induced by proinflammatory stimuli such as interleukin-1 (IL-1), tumor necrosis factor α (TNF-α), growth factors, and endotoxin lipopolysaccharide (LPS).[4–7] The increased levels of PGs produced by the newly formed COX-2 cause the pathologic symptoms of inflammation.[4–8]

Therefore, specific COX-2 inhibitors display efficacy as analgesic and antiinflammatory agents without causing GI damage and antiplatelet activity demonstrated by traditional nonselective NSAIDs.[4–8] The decreased GI side effect profile may explain the rapid acceptance of the first two COX-2 inhibitors recently marketed, celecoxib (SC-58635, 4-[5-(4-methylphenyl)-3-(trifluoromethyl)-1H-pyrazol-1-yl]benzenesulfonamide, **1**)[9] and rofecoxib (MK-0996, 4-[4-(methylsulfonyl)phenyl]-3-phenylfuran-2(5H)-one, **2**) (Chart 1).[10] Selective COX-2 inhibitors, due to their higher therapeutic index, can be studied at levels in excess of their therapeutic, antiinflammatory dosage. Consequently, many new areas of research have become available. Pivotal preclinical and clinical research in the chemoprevention and treatment of cancer and the treatment of Alzheimer's disease is also in progress.[11–14]

1,5-Diarylpyrazole derivatives including celecoxib (**1**), a market-launched antiinflammatory drug,[9,15] could selectively inhibit COX-2. Their structures and activities are listed in Table 1 (compounds **3–42**). Some of these inhibitors show potent inhibitory activities toward COX-2; compound **19** (Table 1) is a typical example among them (IC₅₀ values for COX-2 and COX-1 are, respectively, 3.7 nM and 6.33 μM).[15] In 1999, the three-dimensional (3D) structures of murine COX-2 and ovine COX-1 complexing, respectively, with SC-558 (**43**) and flurbiprofen (**44**) were solved by X-ray crystallogra-

---

* To whom correspondence should be addressed. Tel: +86-21-64318401. Fax: +86-21-64370269. E-mail: jiang@iris3.simm.ac.cn, jhshen@mail.shcnc.ac.cn.

Chart 1
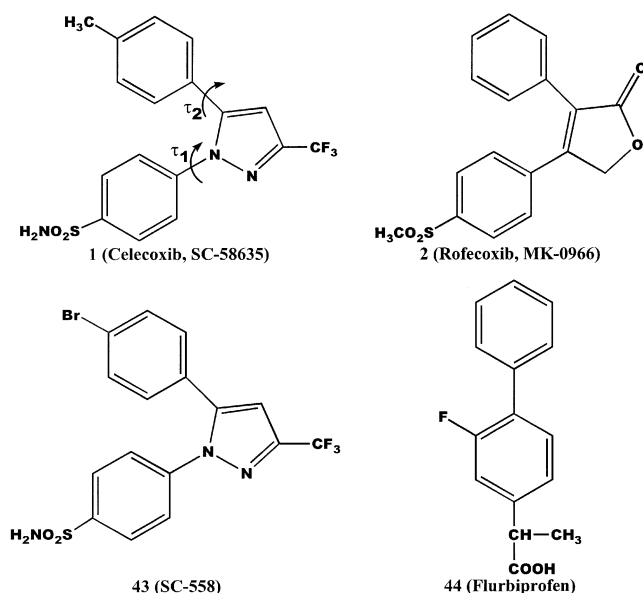
phy.[16,17] This provided a solid foundation for designing new selective COX-2 inhibitors. 1,5-Diarylpyrazole analogues show strong potency and good enzyme selectivity in inhibiting COX-2.[9,15] Structure−activity relationship (SAR) studies indicated that the polar sulfonyl moiety of 1,5-diarylpyrazoles, which may fit into a relatively polar side pocket of COX-1 or COX-2, is a very important pharmacophore element.[18−20] The origins of binding affinity for several analogues of 1,5-diarylpyrazole have been explored by P. Price and W. L. Jorgensen[20,21] employing docking, Monte Carlo (MC) simulation, and free energy perturbation (FEP) approaches. Some clues from simple quantitative SAR (QSAR) studies on diarylheterocyclic derivatives were obtained by the selection of positional substituents.[22] The sophisticated structure-based computational approaches, such as MC simulation[21] and FEP techniques,[23] are approved to be valuable for accurately predicting binding affinity but could not be extended to predict the binding affinities for a large set of molecules due to time constraints. The QSAR approaches are not direct in exploring the binding mechanism between ligands and receptors. Automated molecular docking can predict the binding affinity very quickly with an empirical scoring method.[24,25] In addition, automated molecular docking can be applied in constructing the predictive model for a series of molecules. The binding conformations of the ligands and their alignment in the active site of the receptor can be used for generating 3D QSAR models, which can be further applied in activity prediction at a faster speed.[26,27] Therefore, in this paper, we studied the binding models of 1,5-diarylpyrazole analogues against COX-2 and the COX-2/COX-1 selectivity using automated molecular docking approaches. Following the docking result, 3D QSAR models were constructed by using approaches of comparative molecular field analysis (CoMFA)[28] and comparative molecular similarity analysis (CoMSIA).[29] To the best of our knowledge, no previous effort has been carried out to seek new insight into the relationship of the structure information with the inhibitory potency and selectivity of 1,5-diarylpyrazole compounds employing combined computational methods of automated molecular docking with 3D QSAR approaches. The aim of the present research is to (i) demonstrate the common binding model of 1,5-diarylpyrazole compounds with COX-2 and COX-1, (ii) predict the binding free energy relative to the inhibitory potency and selectivity of these compounds, and (iii) elucidate the structural features associated with the chemical modifications and explain the SAR data for COX-2 inhibitors. Furthermore, the important goal is to obtain stable and predictive QSAR models involving the main intermolecular interactions between inhibitors and COX-2, which can be used in rapidly and accurately predicting the activities of new designed inhibitors.

Computational Details

1. Molecular Docking. The crystal structures of murine COX-2 in complex with **43**[16] and ovine COX-1 in complex with flurbiprofen (**44**)[17] were recovered from the Brookhaven Protein Data Bank (http://www.rcsb.org/pdb/) (entry codes 1prh and 1cx2). The potential of the 3D structures of COX-2 and COX-1 was assigned according to the Amber 4.0 force field with Kollman-all-atom charges encoded in Sybyl 6.7.[30] The initial structures of 40 1,5-diarylpyrazole compounds (compounds **3**−**42** in Table 1) were generated by molecular modeling software Sybyl 6.7.[30] The geometries of these compounds were subsequently optimized using the Tripos force field[31] with Gasteiger−Hückel charges.[31] The method of Powell available in the Maximin2 module encoded in Sybyl 6.7[30] was used for energy minimization using an 8 Å nonbond cutoff and an energy convergence gradient value of 0.005 kcal/(mol Å).

For the reason of tackling the interacting mode of 1,5-diarylpyrazoles (inhibitors) with COX-2 and COX-1 (enzymes), the advanced docking program AutoDock 3.0[24,25] was used to perform the automated molecular docking. The Lamarckian genetic algorithm (LGA)[25] was applied to deal with the inhibitor−enzyme interactions. Briefly, the LGA described the relationship between the inhibitors and the enzymes by the translation, orientation, and conformation of the inhibitors. These so-called "state variables" were the inhibitors' genotype, and the resulting atomic coordinates together with the interaction and the intramolecular energies were the inhibitors' phenotype. The environmental adaptation of the phenotype was reverse-transcribed into its genotype and became heritable traits. Each docking cycle, or generation, consisted of a regimen of fitness evaluation, crossover, mutation, and selection. A Solis and Wets local search[33] performed the energy minimization on a user-specified proportion of the population. The docked structures of the inhibitors were generated after a reasonable number of evaluations. The whole docking operation could be stated as follows.

First, the enzyme molecules were checked for polar hydrogens and assigned for partial atomic charges, the PDBQs file was created, and the atomic solvation parameters were also assigned for the macromolecules. Meanwhile, all of the torsion angles of the inhibitors in order to be explored during molecular docking were defined. This allowed the conformational search of inhibitors during the process of docking.

Second, the 3D grid was created by the AutoGrid algorithm[25] to evaluate the binding energies between the inhibitors and the enzymes. In this stage, the COX-2

Table 1. Structures of 1,5-Diarylpyrazole Compounds and their Inhibitory Activities
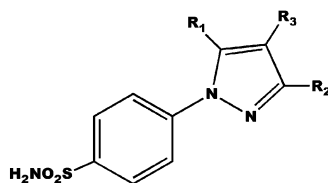
compd	R_1	R_2	R_3	pIC$_{50}$[a] COX-1	COX-2
3	phenyl	CF$_3$	H	4.26	7.50
4	2-F-phenyl	CF$_3$	H	4.53	7.24
5	4-F-phenyl	CF$_3$	H	4.59	7.39
6	2-Cl-phenyl	CF$_3$	H	4.50	7.25
7	2-Me-phenyl	CF$_3$	H	4.47	7.16
8	4-Me-phenyl	CF$_3$	H	4.82	7.40
9	4-CN-phenyl	CHF$_2$	H	<4	4.53
10	4-COOH-phenyl	CHF$_2$	H	<4	4.33
11	4-NO$_2$-phenyl	CF$_3$	H	<4	5.58
12	4-SMe-phenyl	CF$_3$	H	5.92	8.05
13	2-NMe$_2$-phenyl	CF$_3$	H	<4	4.84
14	4-NHMe-phenyl	CF$_3$	H	4.86	7.80
15	4-CH$_2$OH-phenyl	CF$_3$	H	<3	4.03
16	4-COOH-phenyl	CF$_3$	H	<3.60	4.95
17	3-chloro-4-methoxy-phenyl	CHF$_2$	H	4.56	7.57
18	3-methyl-4-methoxy-phenyl	CF$_3$	H	4.81	8.03
19	3-methyl-4-(methylthio)-phenyl	CF$_3$	H	5.20	8.43
20	3-fluoro-4-(dimethylamino)-phenyl	CF$_3$	H	5.42	8.24
21	3-chloro-4-(methylamino)-phenyl	CF$_3$	H	4.11	7.57
22	3,5-dichloro-4-methoxy-phenyl	CHF$_2$	H	4.11	7.68
23	3,5-difluoro-4-methoxy-phenyl	CHF$_2$	H	4.20	6.46
24	3,4-dichloro-phenyl	CF$_3$	H	4.76	7.82
25	2,4-dimethyl-phenyl	CF$_3$	H	4.09	6.92
26	2-pyridyl	CF$_3$	H	4.03	4.34
27	3-pyridyl	CF$_3$	H	<4	4.35
28	4-pyridyl	CF$_3$	H	3.68	4.19
29	5-chloro-2-thienyl	CF$_3$	H	5.33	7.59
30	5-(2,3-2H-benzofuran)	CF$_3$	H	5.92	7.68
31	phenyl	CH$_3$	H	<4	4.20
32	4-Cl-phenyl	CF$_3$	Cl	7.19	8.28
33	4-Cl-phenyl	CF$_3$	Me	6.03	7.66
34	4-Cl-phenyl	CF$_3$	Et	4.53	7.55
35	phenyl	CF$_3$	OMe	<4	7.10
36	phenyl	H	CH$_3$	<4	4.33
37	4-CH$_3$-phenyl	H	CN	<4	7.12
38	4-Cl-phenyl	H	SO$_2$Me	4.28	4.70
39	phenyl	H	NH$_2$	5.29	4.53
40	4-Cl-phenyl	CN	Cl	6.85	8.00
41	4-Cl-phenyl	COOMe	Cl	6.39	6.80
42	4-Cl-phenyl	CONH$_2$	Cl	5.06	5.96
1*	4-Cl-phenyl	CF$_3$	H	4.75	8.00
2*	3-Me-phenyl	CF$_3$	H	4.74	6.96
3*	2-OMe-phenyl	CF$_3$	H	<4	6.54
4*	4-OMe-phenyl	CF$_3$	H	5.59	8.10
5*	3,4-dimethoxy-phenyl	CF$_3$	H	<4	6.22
6*	5-methyl-2-furyl	CHF$_2$	H	<4	5.48
7*	1-cyclohexenyl	CF$_3$	H	<4	7.08
8*	phenyl	CHF$_2$	H	4.47	6.89
9*	4-Cl-phenyl	CH$_2$OCH$_2$Ph	H	5.05	7.54
10*	4-F-phenyl	CN	H	<4	6.47

* Compounds that were not included in the construction of 3D QSAR models. [a] $-$logIC$_{50}$.

or COX-1 was embedded in the 3D grid and a probe atom was placed at each grid point. The affinity and electrostatic potential grid were calculated for each type of atom in the inhibitors. The energetics of a particular inhibitor configuration was found by trilinear interpolation of affinity values and electrostatic interaction of the eight grid points surrounding each of the atoms in an inhibitor.

Third, a series of the docking parameters were set on. Not only the atom types but also the generations and the number of runs for the LGA algorithm were edited

and properly assigned according to the requirement of the Amber force field. The number of generations, energy evaluations, and docking runs were set to 370 000, 1 500 000, and 20, respectively. The kinds of atomic charges were taken as Kollman-all-atom[34] for COX-2 and COX-1 and Gasteiger$-$Hückel[31] for the inhibitors.

Finally, the docked complexes of inhibitor$-$enzyme were selected according to the criteria of interacting energy combined with geometrical matching quality. These complexes were used as the starting conformation

for further energetic minimization and geometrical optimization before the final models were achieved.

2. Binding Affinity Prediction. Typically, three binding energy terms used in the previous versions of AutoDock[24] were included in the score function: the van der Waals interaction represented as a Lennard–Jones 12-6 dispersion/repulsion term, the hydrogen bonding represented as a directional 12-10 term, and the Coulombic electrostatic potential. So, the binding energy of 1,5-diarylpyrazole compounds with COX-2 or COX-1 enzyme could be simply described as the electrostatic, van der Waals, and hydrogen-bonding interaction energy, respectively.

On the basis of the traditional molecular force field model of interaction energy, a new score function at the level of binding free energy was derived and adopted in the version of AutoDock 3.0.[32] Not only the restriction of internal rotors, the global rotation, and the translation were modeled depending on the number of torsion angles of the ligand but also the desolvation upon binding and the hydrophobic effect (solvent entropy changes at solute–solvent interfaces) were calculated. The total binding free energy was empirically calibrated based on the above-stated terms and a set of coefficient factors.[32] Thus, the new score function was sufficient to rank the inhibitors in the different levels of binding affinities, binding free energies, ΔG values, and the corresponding inhibitory constant, K_i values. The same rationale was applied to the system of 1,5-diarylpyrazole compounds and COX-2 or COX-1 in order to evaluate the binding properties more precisely than the traditional molecular mechanics method did, and the total binding free energy and corresponding inhibitory constant between 1,5-diarylpyrazoles and COX-2 or COX-1 were calculated according to the algorithm in the AutoDock 3.0 program.[32]

3. 3D QSAR Analyses. To more fully explore the specific contributions of electrostatic, steric, and hydrophobic effects in the binding of 1,5-diarylpyrazoles to COX-2 and to build predictive QSAR models, CoMFA[28] and CoMSIA[29] studies were performed by using the binding conformations and their alignments at the binding site of the COX-2, which resulted from molecular docking.

3.1. CoMFA. For the CoMFA calculation, steric and electronic field energies were calculated using an sp^3 carbon as the steric probe atom and a +1 charge for the electrostatic probe. Steric and electrostatic interactions were calculated using the Tripos force field with a distance-dependent dielectric constant at all intersections in a regularly spaced (2 Å) grid. The minimum σ (column filtering) was set to 2.0 kcal/mol to improve the signal-to-noise ratio by omitting those lattice points whose energy variation was below this threshold. A cutoff of 30 kcal/mol was adopted, and the regression analysis was carried out using the full cross-validated partial least squares (PLS)[33,34] method (leave one out) with CoMFA standard options for scaling of variables. The final model (noncross-validated conventional analysis) was developed and yielded the highest cross-validated q^2 value with the optimum number of components equal to that yielding the highest q^2.

3.2. CoMSIA. The alignment also served to compute similarity index fields for CoMSIA analysis. In this
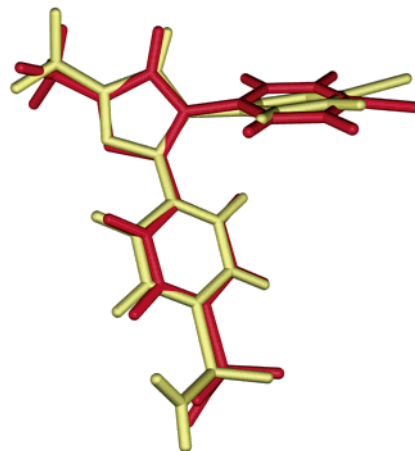
Figure 1. Conformational comparison of SC-558 from the crystal structure (yellow) and that from the AutoDock result (red). It is rendered by the POV-Ray[36] program.

study, three physicochemical properties, steric, electrostatic, and hydrophobic fields, have been evaluated. The steric contribution was reflected by the third power of the atomic radii of the atoms. Electrostatic properties were introduced as atomic charges resulted from molecular docking. An atom-based hydrophobicity was assigned according to the parametrization developed by Viswanadhan et al.[35] The lattice dimensions were selected with a sufficiently large margin (>4 Å) to enclose all aligned molecules. Any singularities were avoided at atomic positions in CoMSIA fields because a Gaussian type distance dependence of the physicochemical properties was adopted, thus no arbitrary cutoffs were required. In general, similarity indices, $A_{F,K}$, between the compounds of interest and a probe atom placed at the intersections of the lattice could be calculated with eq 1

$$A_{F,K}^q(j) = -\sum_{i=1}^{n} w_{probe,k}\, w_{ik}\, e^{-ar_{iq}^2} \tag{1}$$

where q represents a grid point; i is the summation index over all atoms of the molecule j under computation; w_{ik} is the actual value of the physicochemical property k of atom i; and $w_{probe,k}$ is the value of the probe atom. In the present study, similarity indices were computed using a probe atom ($w_{probe,k}$) with charge +1, radius 1 Å, hydrophobicity +1, and attenuation factor α 0.3 for the Gaussian type distance. The statistical evaluation for the CoMSIA analyses was performed in the same way as described in CoMFA. All of the calculations were performed on a Silicon Graphics Indigo XZR 10000 workstation.

Results and Discussion

1. Interacting Model with COX-2. 1.1. Inhibitor's Conformation. The AutoDock predicted conformation of SC-558 (**43**) is shown in Figure 1 with the X-ray crystallographic obtained conformation[16] superposition. The root mean square deviation (RMSD) between these two conformations is ~0.17 Å, indicating that the parameter set for the AutoDock simulation is reasonable to reproduce the X-ray structure. The AutoDock method

(A)

(B)
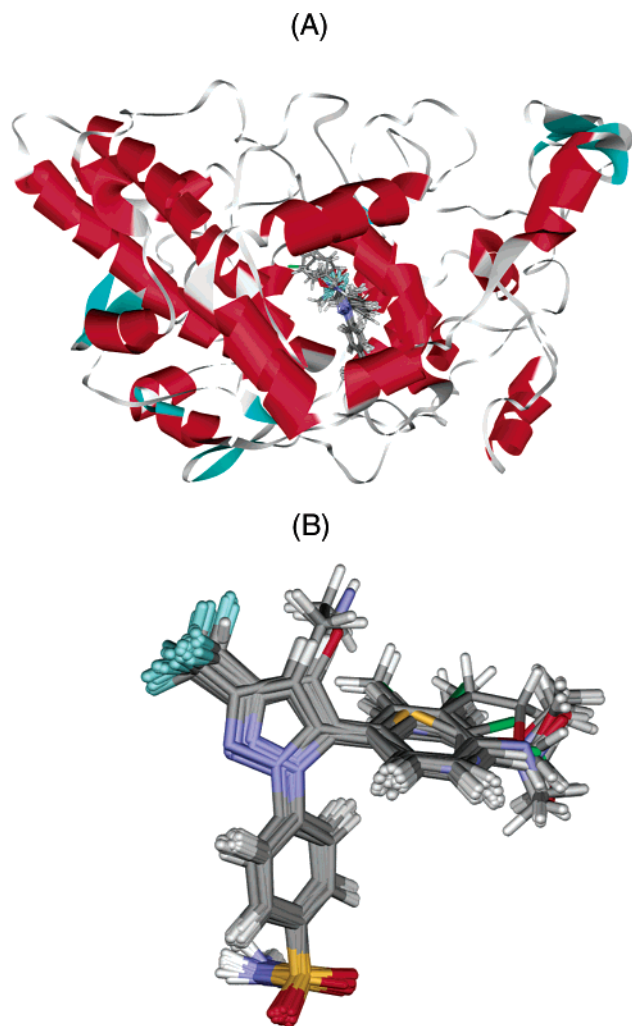
Figure 2. (A) Three-dimensional structural model of 1,5-diarylpyrazole compounds/COX-2 complex. (B) Probable binding conformations of 1,5-diarylpyrazole compounds and their alignment in the binding site of COX-2.

Table 2. Geometrical Parameters of Binding Conformations of 1,5-Diarylpyrazole Compounds and RMSD Values as Compared with SC-558 from Crystal Structure 1cx2[13]

compd	τ_1 (°)	τ_2 (°)	RMSD	compd	τ_1 (°)	τ_2 (°)	RMSD
3	120.1	151.2	0.147	28	118.9	140.5	0.187
4	125.9	148.2	0.188	29	132.1	144.7	0.206
5	124.1	147.1	0.154	30	129.3	143.0	0.188
6	123.3	148.7	0.145	31	122.7	140.7	0.183
7	120.7	149.6	0.174	32	119.0	145.1	0.167
8	124.4	146.9	0.185	33	121.9	143.9	0.173
9	122.0	148.1	0.154	34	119.6	148.0	0.155
10	120.3	144.4	0.193	35	123.1	144.7	0.205
11	112.9	143.9	0.181	36	117.2	144.6	0.161
12	123.3	151.4	0.169	37	116.5	142.9	0.176
13	130.4	144.8	0.171	38	97.7	134.1	0.168
14	114.8	153.5	0.171	39	115.4	141.3	0.114
15	115.9	143.7	0.178	40	113.7	143.2	0.172
16	109.8	152.2	0.174	41	111.3	144.5	0.178
17	123.6	148.0	0.196	42	112.4	130.2	0.138
18	123.0	145.8	0.194	1*	117.4	149.2	0.155
19	101.9	134.8	0.142	2*	121.2	148.2	0.153
20	114.8	149.4	0.194	3*	120.1	149.9	0.154
21	126.1	143.0	0.187	4*	121.0	151.1	0.172
22	126.4	157.1	0.136	5*	132.2	144.9	0.216
23	121.7	152.9	0.144	6*	143.0	142.8	0.191
24	128.3	143.5	0.181	7*	102.4	149.8	0.197
25	120.8	144.1	0.167	8*	122.2	146.0	0.201
26	115.0	143.2	0.161	9*	125.7	150.0	0.187
27	121.5	141.3	0.183	10*	115.6	150.3	0.161
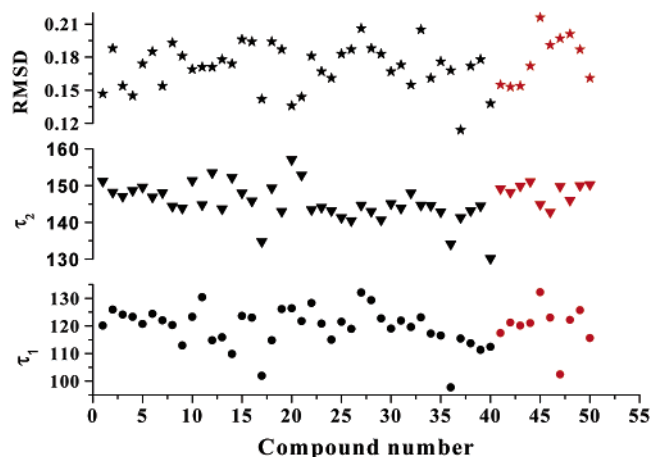
Figure 3. Geometrical parameters (τ_1 and τ_2) and RMSD values of 1,5-diarylpyrazole as compared with SC558; red-colored points are of the testing set compounds.[37]

and the parameter set could be extended to search the enzyme binding conformations for other inhibitors accordingly. Figure 2A shows the 3D model of 1,5-diarylpyrazole–COX-2 complexes, and Figure 2B illustrates the probable binding conformational alignment for the 40 1,5-diarylpyrazoles extracted from the Auto-Dock diarylpyrazole–COX-2 complexes. The main conformational difference between the diarylpyrazoles and the SC-558 (**43**) could be represented as the two torsion angles (τ_1 and τ_2 in formula 1) and the RMSD values based on the parts of similar structure. These data are summarized in Table 2 and shown in Figure 3. Just like SC-558 (**43**) cocrystallized with COX-2,[16] 1,5-diaryl-pyrazoles are located in the center of the typical binding pocket of COX-2 and share some common binding features for each other. All of the 1,5-diarylpyrazoles are bound in the active site of COX-2 in a similar conformation of SC-558 (**43**) in the X-ray structure cocrystallized with COX-2 (Figure 2), and the binding conformations of 1,5-diarylpyrazoles could be aligned quite well overall.

1.2. Hydrogen-Bonding Interactions. Figure 4 generally represents the interacting model of compound **19** (the most potent inhibitor among the 40 diaryl-pyrazoles) with COX-2 derived by the LIGPLOT pro-

gram.[38] Following a similar binding pattern, hydrogen bonding is one important characteristic of the interaction between the 1,5-diarylpyrazoles and the COX-2 (Figures 4). There are several hydrogen bonds formed between the 1,5-diarylpyrazoles and some residues in COX-2. The amido in the sulfonamide group of **19** acts as a donor to form hydrogen bonds with O atoms of Leu352 and Ser353 and O^ϵ of Gln192 (Figure 4). One O atom in the sulfonamide of compound **19** acts as an acceptor to form a hydrogen bond with the N^ϵ atom of His90. This hydrogen bond network in the catalytic site of COX-2 must play a vital role in determining the level of binding affinities for 1,5-diarylpyrazoles with COX-2, and this may be the important reason why these compounds could inhibit the COX-2 potentially. The F atom in the trifluoromethyl ($-CF_3$) of compound **19** acts as an acceptor to form a hydrogen bond with the $-N^{\eta 1}H$ group of the Arg120 side chain, and this negatively electrostatic group ($-CF3$) may also interact with the
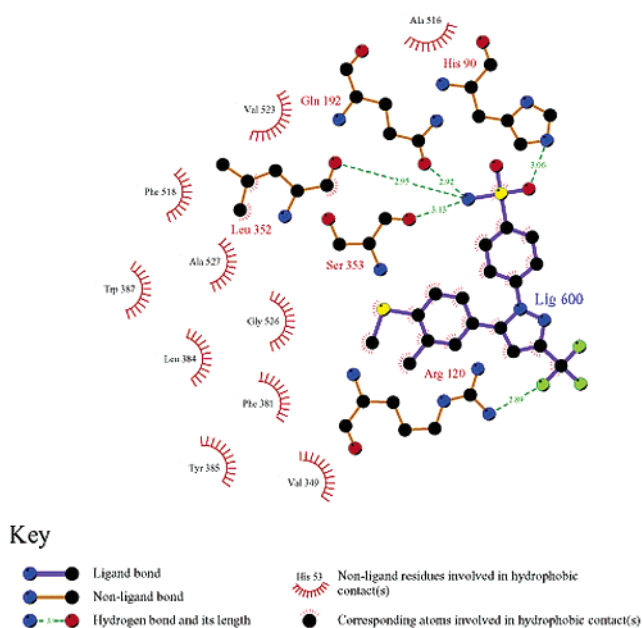
Figure 4. Two-dimensional representation for the interacting mode of compound **19** with COX-2; it is drawn using the LIGPLOT[38] program.

positively charged carbamidine end of the Arg120 side chain through strong electrostatic interaction. The hydrogen-bonding and the electrostatic interaction act as an "anchor", intensely determining the 3D space position of the arylcyclic and heterocyclic moieties in the binding pocket and facilitating the hydrophobic interaction of the aromatic and heterocyclic rings with the side chains of residues Ala527, Gly526, Phe518, Ala516, Trp387, Tyr385, Leu384, Phe381, Leu352, and Val349 in COX-2 (Figure 4).

1.3. Interactions of Substituents. The R$_1$ groups (Table 1, the bromophenyl of **43**) of all of the 40 1,5-diarylpyrazole compounds bind with the side chains of residues Leu352, Phe381, Leu384, Tyr385, Trp387, Val523, Gly526, and Ala527 of COX-2 through not only hydrophobic interaction but also electrostatic interaction to some extent (Figure 4). The side of the binding site bordered by Tyr385 is quite sterically restricted. In general, smaller substituents are generally better binders (Figure 4). Thus, compounds **8** and **12** are, respectively, more potent compounds **15** and **18**.

The R$_2$ groups (Table 1, trifluromethyl of **43**) are bound in an adjacent pocket formed by Met113, Val116, Val349, Tyr355, Leu359, and Leu531 through hydrophobic interaction. It tended to be very tolerant of a variety of functionalities and seemed to have very few steric restrictions; therefore, the trifluoromethyl and difluoromethyl substituents provided superior potencies and selectivity. This is the reason why the inhibitory activities of compounds have the order of **32** > **40** > **41** > **42**.

The R$_3$ groups (Table 1, hydrogen of **43**) interact with the side chains of residue Ala527 through a hydrophobic interaction (Figure 4). Smaller substituents are also generally better binders because the space around the binding site is relatively small, which is bordered by Arg120, Gly526, Tyr385, Leu384, and Phe381. Thus, the inhibitory activities of the inhibitors have the order of **1*** > **32** > **33** > **34** > **37** > **38**.

The phenyl ring of the entire phenylsulfonamide moiety binds with the side chains of residues Leu352, Tyr355, Ala516, Phe518, and Val523 and the backbone of Ser353 through not only hydrogen-bonding but also hydrophobic interactions. Beyond this hydrophobic pocket, the sulfoamide group extends into a relatively polar side pocket that is somewhat restricted in COX-1, as has been indicated by Price and Jorgensen.[20] On the basis of site-directed mutagenesis experiments,[39,40] the primary factor contributing to the COX-2 selectivity of **1** and related 1,5-diarylpyrazoles is the substitution of Ile523 in COX-1 by valine in COX-2. However, the nearby Arg513His mutation may also contribute to the inhibitor's selectivity.[39-40] Crystal structure data suggest that this residue difference improves access of the sulfonamide to a side pocket.[16] It is dubious for the orientation and conformation of the sulfonamide that two X-ray structures of SC-558 bound to COX-2 (1cx2 and 6cox) formed in different space groups revealed two different orientations of the sulfonamide.[16] Price and Jorgensen concluded that the sulfonamide moiety adopts the orientation and conformation as that in 6cox.[16, 20] The AutoDock results reveal that the sulfonamide group could bind in several conformations than suggested by the crystal structures. To quantify the energetic preference, a conformational search was performed on the sulfonamide of SC-558 in the COX-2 binding site environment by using the systematic search routine of Sybyl 6.7.[30] The result indicates that conformation of the sulfonamide predicted by AutoDock is lower in energy by 1.52 kcal/mol than the crystal structure 1cx2. The conformational search also indicates that the binding pocket has enough space for the sulfonamide group rotating around its C—S bond. As shown in Figure 4, our AutoDock conformation (orientation) of the sulfonamide group increases the hydrogen bonding between the inhibitors and the COX-2, forming four additional hydrogen bonds with His90, Gln192, Leu352, and Ser353 (Figure 4 and above discussion); no more such hydrogen bonds are found in the X-ray structure of 1cx2.[16] The binding free energy between SC-558 (**43**) and COX-2 estimated based on the crystal structure is −11.35 kcal/mol, and that estimated based on the AutoDock structure is −12.35 kcal/mol. Therefore, the additional hydrogen bonding also reflects in the binding affinity increasing by about 1 kcal/mol.

2. Correlation between Binding Free Energy and Inhibitory Activity. Table 3 lists the calculated binding free energies of 1,5-diarylpyrazoles with COX-2, and Figure 5 shows the relationship between the calculated binding free energies and the inhibitory activities, IC$_{50}$ values. Satisfied that the 3D structures of 1,5-diarylpyrazole−COX-2 complexes were practically reasonable, the multiple regression analysis (MRA)[41] was performed to explore whether the inhibitory potencies of 1,5-diarylpyrazole compounds could be correlated with the energetic data. The regression equation was obtained for the inhibitory potencies, −logIC$_{50}$ values, represented as pIC$_{50}$ values, using the total binding free energies, ΔG, as the sole descriptor variable. A good correlation was found between the inhibitory activities and the calculated binding free energies (eq 2), also shown in Figure 5A. This relationship suggests that those potential COX-2 inhibitors exhibiting stronger

Table 3. Predicted Binding Free Energy (kcal/mol), the Inhibition Constant (K_i Values) with COX-2 and COX-1, Respectively, and the Experimental Activity (pIC_{50}, $-\log IC_{50}$) of 40 1,5-Diarylpyrazole Compounds

compd	pIC_{50}^{cox-2} [a]	pIC_{50}^{cox-1} [b]	ΔG^{cox-2} (kcal/mol)	ΔG^{cox-1} (kcal/mol)	K_i^{cox-2}	K_i^{cox-1}	selectivity exp[c]	selectivity pred[d]
3	7.50	4.26	−11.7	−6.23	2.65×10^{-9}	2.17×10^{-5}	3.24	3.91
4	7.24	4.53	−11.8	−7.24	2.22×10^{-9}	4.89×10^{-6}	2.71	3.34
5	7.39	4.59	−11.9	−6.87	1.80×10^{-9}	9.29×10^{-6}	2.79	3.71
6	7.25	4.50	−12.3	−5.98	1.06×10^{-9}	4.10×10^{-5}	2.75	4.59
7	7.16	4.47	−12.2	−6.86	1.25×10^{-9}	9.36×10^{-6}	2.69	3.87
8	7.40	4.82	−12.5	−7.44	7.34×10^{-10}	3.54×10^{-6}	2.57	3.68
9	4.53	<4	−11.4	−6.20	4.73×10^{-9}	2.87×10^{-5}	>0.527	3.78
10	4.33	<4	−11.4	−6.25	4.26×10^{-9}	2.63×10^{-5}	>0.330	3.79
11	5.58	<4	−12.2	−6.09	1.12×10^{-9}	3.41×10^{-5}	>1.58	4.48
12	8.05	5.92	−12.6	−10.6	5.48×10^{-10}	1.81×10^{-8}	2.12	1.52
13	4.84	<4	−12.2	−6.36	1.23×10^{-9}	2.19×10^{-5}	>0.845	4.25
14	7.80	4.86	−12.4	−5.86	7.86×10^{-10}	5.03×10^{-5}	2.94	4.81
15	4.03	<3	−11.4	−5.70	4.28×10^{-9}	6.59×10^{-5}	1.03	4.19
16	4.95	<3.60	−12.2	−3.70	1.22×10^{-9}	0.00	>1.35	
17	7.57	4.56	−12.8	−7.26	4.08×10^{-10}	4.75×10^{-6}	3.01	4.07
18	8.03	4.81	−12.9	−7.13	3.30×10^{-10}	5.90×10^{-6}	3.22	4.25
19	8.43	5.20	−13.1	−8.06	2.36×10^{-10}	1.23×10^{-6}	3.23	3.72
20	8.24	5.42	−13.4	−7.78	1.60×10^{-10}	2.00×10^{-6}	2.82	4.10
21	7.57	4.11	−13.4	−4.55	1.45×10^{-10}	4.61×10^{-4}	3.46	6.50
22	7.68	4.11	−13.1	−4.27	2.70×10^{-10}	7.36×10^{-4}	3.56	6.44
23	6.46	4.20	−12.6	−6.62	5.85×10^{-10}	1.41×10^{-5}	2.26	4.38
24	7.82	4.76	−13.2	−7.12	2.18×10^{-10}	6.00×10^{-6}	3.06	4.44
25	6.92	4.09	−13.0	−7.22	3.07×10^{-10}	5.08×10^{-6}	2.83	4.22
26	4.34	4.03	−11.3	−6.63	5.53×10^{-9}	1.38×10^{-5}	0.311	3.40
27	4.35	<4	−11.3	−8.68	5.46×10^{-9}	4.36×10^{-7}	>0.347	1.90
28	4.19	3.68	−11.2	−4.55	6.26×10^{-9}	4.61×10^{-4}	0.509	4.87
29	7.59	5.33	−11.7	−8.02	2.66×10^{-9}	1.39×10^{-6}	2.26	2.72
30	7.68	5.92	−13.2	−8.11	2.03×10^{-10}	1.14×10^{-6}	1.76	3.75
31	4.20	<4	−11.2	−6.64	6.50×10^{-9}	1.36×10^{-5}	>0.202	3.32
32	8.28	7.19	−13.1	−12.4	2.53×10^{-10}	8.26×10^{-10}	1.09	0.514
33	7.66	6.03	−13.1	−8.09	2.65×10^{-10}	1.18×10^{-6}	1.63	3.65
34	7.55	4.53	−13.3	−7.17	1.70×10^{-10}	5.53×10^{-6}	3.03	4.51
35	7.10	<4	−12.0	−6.46	1.58×10^{-9}	1.83×10^{-5}	>3.10	4.06
36	4.33	<4	−10.5	−8.68	1.87×10^{-8}	4.34×10^{-7}	>0.327	1.37
37	7.12	<4	−12.2	−8.26	1.12×10^{-9}	8.88×10^{-7}	>3.12	2.90
38	4.70	4.28	−11.9	−6.8	1.88×10^{-9}	1.04×10^{-5}	0.419	3.74
39	4.53	5.29	−10.8	−7.33	1.13×10^{-8}	4.23×10^{-6}	0.765	2.57
40	8.00	6.85	−12.6	−11.1	5.53×10^{-10}	7.73×10^{-9}	1.15	1.15
41	6.80	6.39	−12.3	−8.03	9.94×10^{-10}	1.31×10^{-6}	0.409	3.12
42	5.96	5.06	−12.0	−6.88	1.74×10^{-9}	9.13×10^{-6}	0.907	3.72
1*	8.00	4.75	−12.5	−6.57	7.49×10^{-10}	1.52×10^{-5}	3.25	4.31
2*	6.96	4.74	−11.9	−6.43	1.83×10^{-9}	1.93×10^{-5}	2.22	4.02
3*	6.54	<4	−11.8	−5.18	2.15×10^{-9}	1.60×10^{-4}	>2.54	4.87
4*	8.10	5.59	−12.2	−6.30	1.07×10^{-9}	2.39×10^{-5}	2.51	4.35
5*	6.22	<4	−11.7	−6.59	2.58×10^{-9}	1.48×10^{-5}	>2.22	3.76
6*	5.48	<4	−11.0	−6.84	8.17×10^{-9}	9.68×10^{-6}	>1.48	3.07
7*	7.08	<4	−11.6	−6.53	3.19×10^{-9}	1.63×10^{-5}	>3.08	3.71
8*	6.89	4.47	−11.4	−7.12	4.14×10^{-9}	6.00×10^{-6}	2.41	3.16
9*	7.54	5.05	−12.5	−7.92	6.94×10^{-10}	$1.58 \times 1 0^{-6}$	2.49	3.36
10*	6.47	<4	−11.7	−6.61	2.58×10^{-9}	1.44×10^{-5}	>2.47	3.75

[a] pIC_{50}^{cox-2} represents $-\log IC_{50}^{cox-2}$. [b] pIC_{50}^{cox-1} represents $-\log IC_{50}^{cox-1}$. [c] COX-2/COX-1 selectivity experimental values, calculated by $\log(IC_{50}^{cox-1}/IC_{50}^{cox-2})$. [d] COX-2/COX-1 selectivity predicted values, calculated by $\log(K_i^{cox-1}/K_i^{cox-2})$.

binding free energies using this paradigm would therefore expect to have greater efficacy toward inhibitory action.

$$- \log IC_{50}cox2 = -12.391 - 1.5488 \times \Delta G \quad (2)$$

$$(n = 40, \ r^2 = 0.648, \ F_{1,38} = 69.961, \ s = 0.229)$$

3. Correlation of COX-2/COX-1 Selectivity. To probe structural and energetic factors of the COX-2/COX-1 selectivity for COX-2 inhibitors, 3D models of the 40 1,5-diarylpyrazoles with COX-1 were also generated using the similar molecular docking methods as described above. The calculated binding free energies are compiled again in Table 3. The regression analysis shows that the inhibitory potencies of COX-1, $-\log IC_{50}$ values, represented as pIC_{50}, correlate well with the total binding free energies, ΔG (eq 3), and this relationship is graphically represented in Figure 5B. Compounds **9**−**11**, **13**, **15**, **16**, **27**, **31**, and **35**−**37** were not included in the regression calculation due to their uncertain values of IC_{50} (Tables 1 and 3).

$$- \log IC_{50}cox1 = 1.7809 - 0.4344 \times \Delta G \quad (3)$$

$$(n = 29, \ r^2 = 0.752, \ F_{1,27} = 81.709, \ s = 0.445)$$

On the basis of the calculated binding free energies and predicted of binding constants (K_i) for 1,5-diarylpyrazoles with COX-2 and COX-1, further analyses were performed for the K_i ratios' logarithm calculation (the values of $\log(K_i^{cox-1}/K_i^{cox-2})$, Table 3) and the statistical regression. A good correlation was found for the $\log(K_i^{cox-1}/K_i^{cox-2})$ and the $\log(IC_{50}^{cox-1}/IC_{50}^{cox-2})$ with the
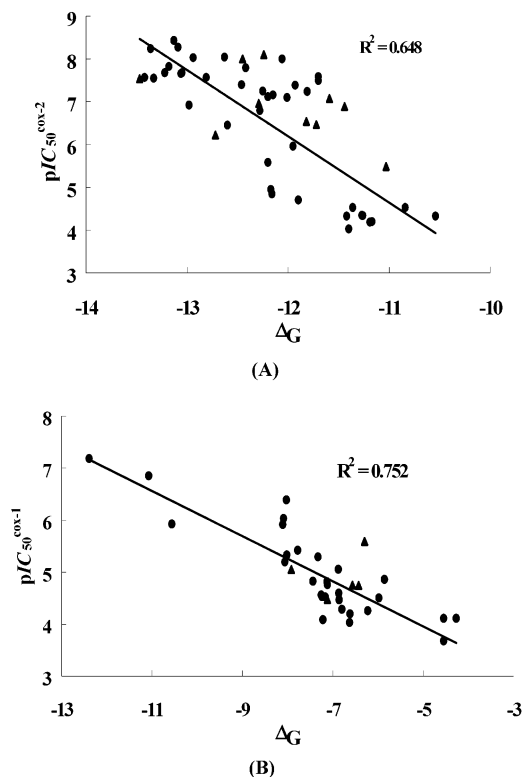
Figure 5. Correlation between the binding free energy (ΔG, kcal/mol, $T = 298.15$ K) of 1,5-diarylpyrazole compounds with COX-2 (A) and COX-1 (B) (●, compounds of the training set; ▲, compounds of the testing set) and the experimental activities ($-\log IC_{50}$).
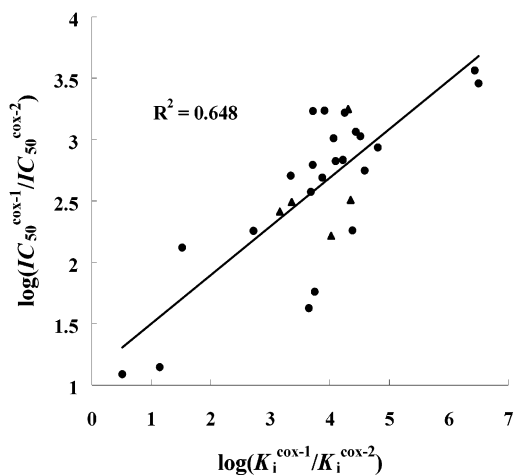
Figure 6. Correlation between $\log(K_i^{cox-1}/K_i^{cox-2})$ and $\log(IC_{50}^{cox-1}/IC_{50}^{cox-2})$ ($T = 298.15$ K) of 1,5-diarylpyrazole compounds (●, compounds of the training set; ▲, compounds of the testing set).

result of $r^2 = 0.648$, and this relationship is indicated in Figure 6. Although compounds **26**, **28**, **38**, **41**, and **42** were not included in the statistical analysis because of their low selectivity to COX-2 (Tables 1 and 3), the correlation between these theoretical and experimental data is indeed satisfactory. Taking into account of all these results, the docking protocol and the binding free energy calculation methods can not only be employed in 3D structural model construction and the binding affinity prediction but also be extended to the prediction of COX-2/COX-1 selectivity if the information of drug action and side effect targets is available.
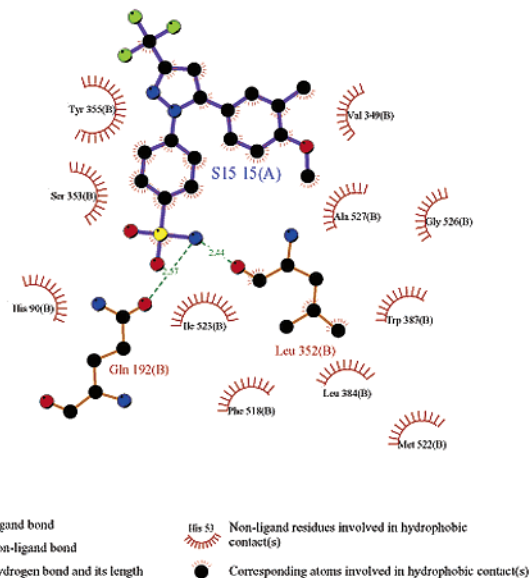
Figure 7. Two-dimensional representative for the interacting model of 1,5-diarylpyrazoles (compound **19** as a representative) with COX-1. It is drawn by LIGPLOT.[38]

As shown in the X-ray structures,[16] the replacement of Ile523 in COX-1 for Val in COX-2 and the sulfonamide moiety of 1,5-diarylpyrazoles is important for COX-2 selectivity, since the additional methylene group in the side chain of Ile523 brings itself unfavorable contacts with phenylsulfonamide substituent, and this kind of steric hindrance makes poor interaction of the sulfonamide group with the side pocket. By docking and MC simulation on 10 diarylpyrazole compounds binding with COX-2 and COX-1, Price and Jorgensen[20] suggested that the COX-2 Val523 to COX-1 Ile replacement must make an unfavorable conformation change of the phenylsulfonamide ring. This viewpoint could be further validated by our molecular docking results for 40 inhibitors binding with COX-2 and COX-1 (Figures 4 and 7). Taking one typical potent COX-2 inhibitor, compound **19**, as an example as shown in Figures 4 and 7, the sulfonamide moiety, a key group related to the selectivity for these compounds, could form two additional hydrogen bonds with COX-2 as compared with the case of COX-1 binding. This great difference in the complex structures brings a direct decrease at the level about 6 kcal/mol in the binding energy with COX-1, and therefore the lower inhibitory activity for COX-1, and certainly originates the COX-2/COX-1 selectivity. Further observation indicates that there are no electrostatic and hydrogen bond interactions of compound **19** with residue Arg120 in the COX-1 complex. A mutagenesis experiment performed by Bhattacharyya[42] indicated that the inhibitor's interaction with the side chain of residue Arg120 was crucial for their binding with COX-1. In accordance with this experimental result, it could be easily deduced that withdrawing the interaction between compound **19** together with its analogues and the side chain of residue Arg120 may be another way to increase COX-2/COX-1 selectivity.

4. 3D QSAR Models. 4.1. CoMFA. Although CoMFA is not able to appropriately describe all of the binding force, being based principally on standard steric and electrostatic molecular fields to model substrate—enzyme interactions, it is still a widely used tool for the

Table 4. Statistical Indexes of CoMFA and CoMSIA Models Based on 40 1,5-Diarylpyrazole Compounds Binding Conformers

	cross-validated		conventional		
	r_{cross}^2	optimal comp	r^2	s	$F_{6,18}$
CoMFA	0.635	6	0.960	0.300	133.031
CoMSIA	0.641	4	0.956	0.134	118.680

Table 5. Predicted Activities (PA) vs Experimental Activities (pIC_{50}, $-logIC_{50}$) and Residues (δ) by CoMFA and CoMSIA

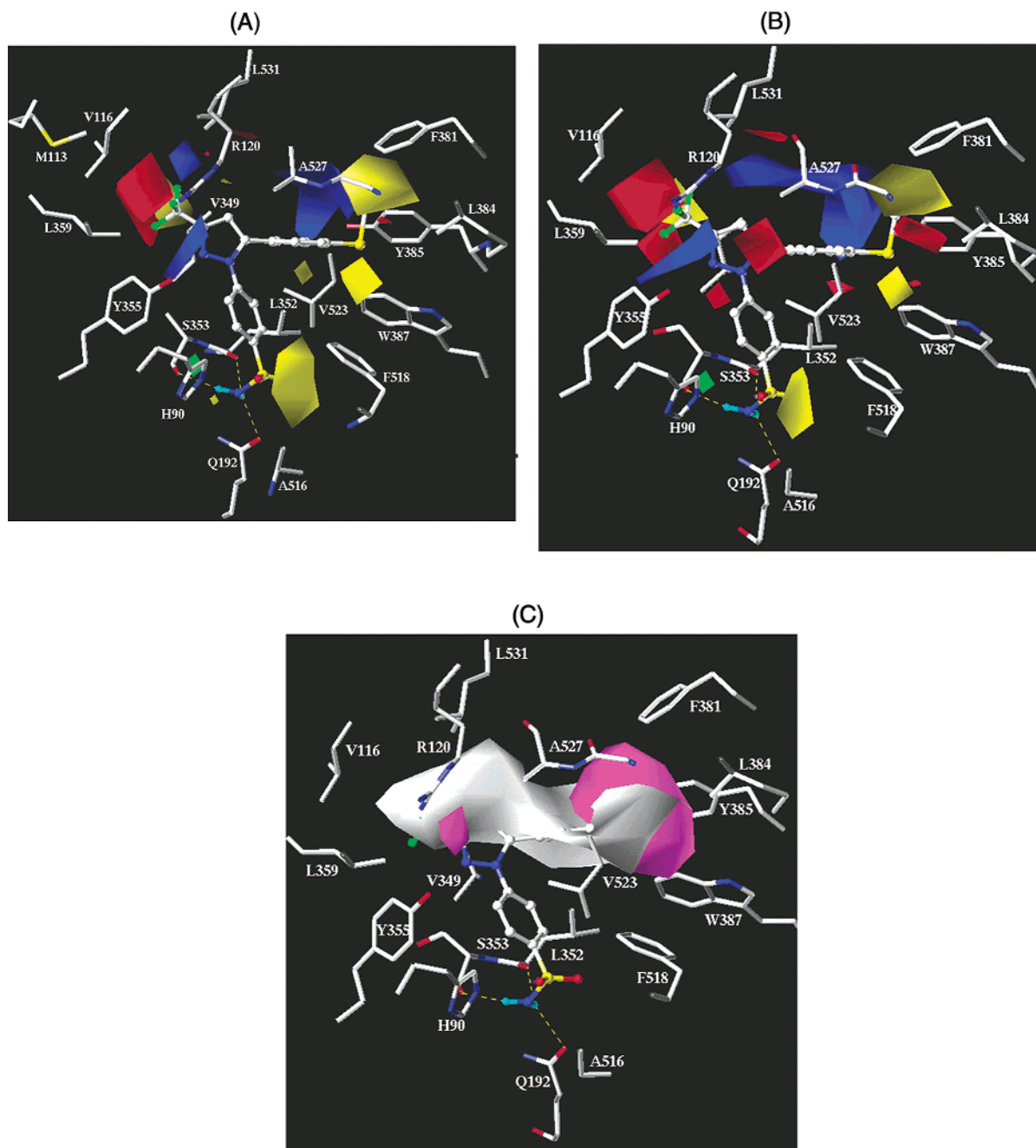|		CoMFA		CoMSIA	
compd	pIC_{50}	PA	δ	PA	δ
3	7.495	6.93	0.56	6.79	0.71
4	7.2366	7.08	0.16	7.03	0.21
5	7.387	7.52	-0.14	7.22	0.17
6	7.252	7.25	0.0032	7.44	-0.19
7	7.16	6.88	0.28	7.02	0.14
8	7.398	7.00	0.40	7.77	-0.37
9	4.5272	5.02	-0.49	4.56	-0.03
10	4.3298	4.33	-0.0019	4.25	0.07
11	5.58	5.47	0.11	5.63	-0.05
12	8.0458	7.36	0.69	7.40	0.64
13	4.8447	4.59	0.26	4.73	0.12
14	7.7959	6.89	0.22	8.10	-0.30
15	4.03012	3.99	0.04	4.15	-0.12
16	4.9508	4.80	0.15	4.93	0.02
17	7.5686	7.33	0.24	6.77	0.79
18	8.0315	8.37	-0.34	8.00	0.03
19	8.4319	8.99	-0.56	8.35	0.09
20	8.2413	8.58	-0.34	8.97	-0.73
21	7.5686	7.45	0.12	7.56	0.01
22	7.6778	7.88	-0.20	7.53	0.15
23	6.4559	6.76	-0.31	6.54	-0.08
24	7.8239	7.75	0.07	8.27	-0.45
25	6.9208	7.04	-0.12	7.38	-0.46
26	4.3411	4.91	-0.57	4.64	-0.29
27	4.3468	4.21	0.14	4.34	0.01
28	4.1891	4.70	-0.51	4.38	-0.19
29	7.585	7.82	-0.23	7.79	-0.21
30	7.6778	7.57	0.11	7.28	0.39
31	4.20204	4.17	0.03	4.78	-0.58
32	8.2757	7.91	0.37	8.01	0.27
33	7.6576	7.64	0.02	7.36	0.30
34	7.5528	7.70	-0.14	7.62	-0.06
35	7.0969	7.13	-0.04	7.07	0.02
36	4.327	4.79	-0.47	4.31	0.02
37	7.1191	6.89	0.23	7.34	-0.22
38	4.7033	4.50	0.20	4.82	-0.12
39	4.5272	4.37	0.16	4.42	0.10
40	8.00	7.96	0.04	7.84	0.16
41	6.7959	6.98	-0.18	6.84	-0.05
42	5.9626	5.92	0.04	5.89	0.08
1*	8.00	7.65	0.35	7.43	0.56
2*	6.96	6.93	0.03	6.88	0.08
3*	6.54	6.78	-0.24	6.74	-0.20
4*	8.09	7.77	0.23	7.43	0.66
5*	6.22	6.44	-0.22	6.57	-0.35
6*	5.48	5.40	0.08	5.95	-0.47
7*	7.08	7.85	-0.77	7.45	-0.37
8*	6.88	6.56	0.32	6.18	0.70
9*	7.54	7.28	0.26	7.61	-0.07
10*	6.47	6.36	0.11	6.70	-0.23
43 (SC558)[13]	8.892	9.12	-0.20	9.04	-0.12

study of QSAR at the 3D level. The major objective of CoMFA analysis about 1,5-diarylpyrazoles is to find the best predictive model within the system. PLS analysis results based on least squares fit are listed in Table 4, which shows that all of the statistical indexes are reasonably high. As listed in Table 4, a CoMFA model with a cross-validated r^2 (q^2) of 0.635 for six components was obtained based on the binding conformations and their alignment in the active site of COX-2. The non-
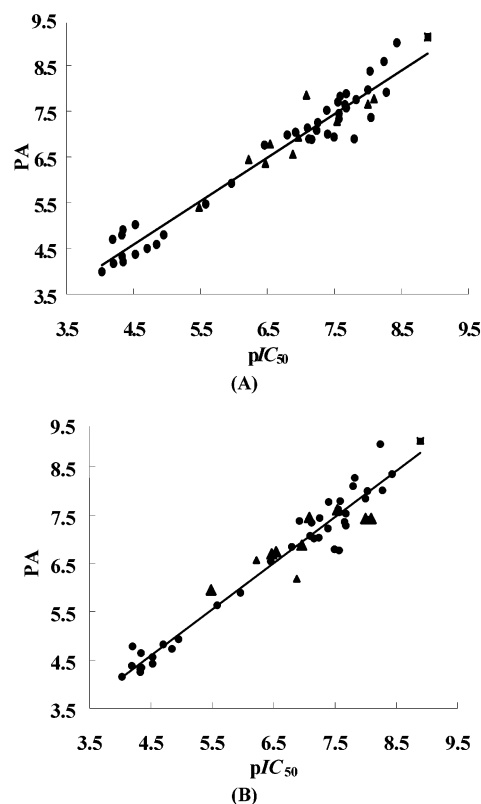
Figure 8. Correlation between predicted activities (PA) by CoMFA (A) and CoMSIA (B) models and the experimental activities of 1,5-diarylpyrazoles (●, compounds of the training set ($r^2 = 0.952$ and 0.956 for the two QSAR models, respectively); ▲, compounds of the testing set ($r^2 = 0.880$ and 0.803 for the two QSAR models, respectively); ■, SC558[16]).

cross-validated PLS analysis was repeated with the optimum number of components, as determined by the cross-validated analysis, to give an r^2 of 0.960, $F = 133$, and the estimated standard error of 0.300. These values indicated a good conventional statistical correlation, and the CoMFA model had a fair predictive ability. The predicted inhibitory activities of these 40 compounds are listed in Table 5 and also shown in Figure 8A, indicating that the fitting power is rational and potent and the predictive ability is satisfactory.

4.2. CoMSIA. CoMSIA analysis results are also summarized in Table 4. A CoMSIA model with an r_{cross}^2 value of 0.641 for four components and a conventional r^2 of 0.956 was obtained. These data demonstrate that the CoMSIA model is also fairly predictive, and the predicted inhibitory potencies of these 40 compounds are listed in Table 5 and also shown in Figure 8B.

4.3. Validation of the QSAR Models. To test the stability and predictive ability of the 3D QSAR results of 1,5-diarylpyrazole compounds, 10 analogous compounds together with compound SC-558 (**43**), which were not included in the construction of CoMFA and CoMSIA models, were selected as a set of testing for the validation (compounds **1***−**10*** in Table 1). The results are also listed in Table 5 and simultaneously shown in Figure 8 (in red triangle and square pattern-labeled symbols), and the predicted $-logIC_{50}$ values (pIC_{50}) are in good agreement with the experimental data in a statistically tolerable error range ($r^2 = 0.880$ and 0.803 for CoMFA and CoMSIA, respectively). To investigate the structural difference of binding mode

Figure 9. Contour maps as compared with the topology of **19**−COX-2 complex. Only the residues within 5 Å around the inhibitor are shown for clarity. (A) CoMFA; (B) the steric and electrostatic field distributions of CoMSIA; and (C) the hydrophobic field distribution of CoMSIA. The residues are represented as sticks, and the inhibitor is shown in ball-and-stick; the dashed lines are the hydrogen bonds formed between inhibitor and COX-2. Sterically favored areas are in green; sterically unfavored areas are in yellow. Positive potential favored areas are in blue; positive potential unfavored areas are in red. Hydrophobic favored areas are in magenta; hydrophilic favored areas are in white.

between the testing set of compounds and the training set, automated molecular docking was performed for the testing set using the same method as that of the training set. The geometrical parameters and the calculated binding free energies for these compounds are also compiled in Tables 2 and 3 and graphically shown in Figures 3 and 5, respectively. As listed in Table 2 and shown in Figure 3, the two torsion angles and the conformational RMSD values as compared with SC-558 (**43**) are in the same levels as that of the training set. Using the AutoDock calculated binding free energies as the independent variables, eq 2 predicted values of $-logIC_{50}$ for the testing compounds have a good cor-

relation with the experimental data, $r^2 = 0.711$ (Figure 5A).

5. CoMFA and CoMSIA Contour Maps Correlate with COX-2 Topology. The QSAR produced by CoMFA, with its hundreds or thousands of terms, was usually represented as 3D "coefficient contour". It shows regions where variations of steric or electrostatic nature in the structural features of the different molecules contained in the training set lead to increases or decreases in the activity. The CoMFA steric and electrostatic fields for the analysis based on the alignments of the binding conformations are presented as contour plots in Figure 9A. To aid in visualization, compound

19 is displayed in the maps. In general, the color polyhedra in the map surrounded all lattice points where the QSAR strongly associated changes in the compounds' field values with changes in biological potency. The CoMFA contour plots show green-colored regions where increased steric bulk is associated with enhanced activity and yellow-colored regions where increased steric bulk is associated with decreased activity. A big region of yellow contour near the sulfonamide moiety suggests that there is an unfavorable steric region relating to the accessibility of the compounds to the COX-2 side pocket. Many COX-2 inhibitors have a part of the structure that exploits binding within the COX-2 side pocket (often via sulfonyl, sulfone, or sulfonamide groups) to achieve selectivity. Another two yellow contours near the 3,5-substituted nonsulfonamide-containing phenyl moiety suggest that they are unfavorable steric regions. It is obvious that the binding site near residue Tyr385 is quite sterically restricted. The third yellow contour near the trifluoromethyl moiety suggests that bulk groups are not beneficial to the inhibitory activity. Regions where increased positive charge is favorable for inhibitory activity are indicated in blue, while regions where increased negative charge is favorable for activity are indicated in red. A red polyhedral near the trifluoromethyl moiety indicates that electron-rich groups are beneficial to the inhibitory activity.

The steric and electrostatic fields of CoMSIA, as shown in Figure 9B, are generally in accordance with the field distribution of CoMFA maps (Figure 9A). Furthermore, the hydrophobic analysis of CoMSIA, based on the atomic hydrophobicity distribution, could demonstrate more clearly the hydrophobic interactions between the 1,5-diarylpyrazole analogues with COX-2. For the hydrophobic maps of CoMSIA, contour plots show magenta-colored regions where increased hydrophobic interaction is associated with enhanced activity and white-colored regions where increased hydrophilic interaction is associated with increased activity. As shown in Figure 9C, the white-colored polyhedral around the upper part of compound **19** indicates that these structural moieties interact with the side chains of residues at the binding site of COX-2 through hydrophilic interaction. This interaction model coincides with the hydrophilic property of the side chains of the residues around this part, especially obvious around residue Arg120. In addition, the magenta-colored polyhedral near the right end of compound **19** illustrates that the phenyl ring group interacts with the side chains of the hydrophobic residues in the side pocket around Tyr385. The consistency between the CoMSIA field distributions and the structural topological properties of the COX-2 binding site demonstrates the reasonability of the CoMSIA result.

Combining the CoMFA and CoMSIA contour maps with the 3D structural topology of the COX-2 binding site, several insights into the binding of 1,5-diaryl-pyrazoles with COX-2, which are described in the Interaction Mechanism section, can also readily be observed from the CoMFA and CoMSIA maps. Not only does the field property coincide perfectly with the environmental characteristics of the binding pocket but also indication for some further structural modification of 1,5-diarylpyrazole compounds could be found. Most of the amino acids around the 1,5-diarylpyrazole compounds in the binding pocket are hydrophobic in nature (Figures 4 and 9). This is inconsistent with the CoMFA and CoMSIA results about the relative field contributions. The colored polyhedrals of CoMFA and CoMSIA located in the cavity of the binding pocket are direct indexes for the kinds and magnitude of the substituents in the process of 1,5-diarylpyrazole analogues synthesis.

Conclusions

We have predicted not only the binding conformations but also the binding free energies of 1,5-diarylpyrazole compounds to COX-2 and COX-1 employing the LGA algorithm of AutoDock. Results indicate that the binding free energies of 1,5-diarylpyrazole compounds calculated by this method correlate well with the reported inhibitory activities against COX-2 and COX-1, and the modeling results provide a satisfactory explanation for the binding mechanism of 1,5-diarylpyrazole compounds with COX-2 and for the COX-2/COX-1 selectivity. Similar to the results of Price and Jorgensen,[20] our AutoDock simulation suggests that the sulfonamide in the COX-2 binding site adopts a different binding orientation and conformation from the crystal structure, which is beneficial to hydrogen-bonding interaction with COX-2. Beside the steric constraint by the Val/Ile replacement at position 523 in COX-1, the COX-2/COX-1 selectivity may also be resulted from the weak hydrogen-bonding interaction of the sulfonamide with COX-1 (Figures 4 and 7). On the basis of the binding conformations of 1,5-diarylpyrazole compounds, we have developed stable and predictive 3D QSAR models with acceptable r_{cross}^2 values by undertaking CoMFA and CoMSIA techniques, and these models could be mapped back to the 3D topology of the binding site of the wild-type enzyme.

Understanding protein−ligand interactions is essential for designing novel synthetic candidates, while those interactions are difficult to describe. Structure-based design is focused on the elucidation of enzyme−substrate interactions but does not always lead to predictive models. On the other hand, 3D QSAR results based on CoMFA and CoMSIA allow focus on those regions, where steric, electronic, or hydrophobic effects play a dominant role in ligand−receptor interactions. These models are usually built using alignment rules, which are not always similar to the bioactive conformation. In this study, we successfully combined with these two approaches: the complex 3D model of diarylpyrazole compounds with COX-2 was derived by AutoDock 3.0 and predictive 3D QSAR models were derived by using alignment conformations extracted directly from the 3D models of the inhibitor−protein complex. This leads to a better understanding of important protein−ligand interactions and thus provides guidelines for ligand design plus a predictive model for scoring novel synthetic candidates. The predictive activity from 3D QSAR and their consistency to inhibit COX-2 activities indicate the validity of those models.

References

(1) Dannhardt, G.; Kiefer, W. Cyclooxygenase inhibitors-current status and future prospects. *Eur. J. Med. Chem.* **2001**, *36*, 19−126.

(2) Carter, J. S. Inhibitors of cyclooxygenase-2: November 1999-April 2000. *Exp. Opin. Ther. Pat.* **2000**, *10* (7), 1011−1020.

(3) Talley, J. J. Selective Inhibitors of Cyclooxygenase-2 (COX-2). *Prog. Med. Chem.* **1999**, *36*, 201−234.

(4) Marnett, L. Cyclooxygenase mechanisms. *Curr. Opin. Chem. Biol.* **2000**, *4*, 545−552.

(5) Garavito, R. M.; Dewitt, D. L. The cyclooxygenase isoforms: structural insights into the conversion of arachidonic acid to prostaglandins. *Biochim. Biophys. Acta* **1999**, *1441*, 278−287.

(6) O'Banion, M. K. Cyclooxygenase-2: Molecular biology, pharmacology, and neurobiology. *Crit. Rev. Neurobiol.* **1999**, *13* (1), 45−82.

(7) Marnett, L. J.; Kalgutkar, A. S. Cyclooxygenase 2 inhibitors: discovery, selectivity and the future. *Tips* **1999**, *20*, 465−469.

(8) Hawkey, C. J. COX-2 inhibitors. *Lancet* **1999**, *353*, 307−314.

(9) Celecoxib. *Drugs Future* **1997**, *22* (7), 711−714.

(10) (a) Rofecoxib. *Drugs Future* **1998**, *23* (12), 1287−1296. (b) Mehlisch D. R.; Mills, S.; Sandler, M.; et al. Ex vivo assay of cox-2 inhibition predicts analgesic efficacy in post-surgical dental pain with MK-966. *Clin. Pharmacol. Ther.* **1998**, *63*, 167.

(11) Hull, M.; Fiebich, B. L.; Schumann, G.; Lieb, K.; Bauer, J. Antiinflammatory substances-a new therapeutic option in Alzheimer's disease. *Drug Discovery Today* **1999**, *4*, 275−282.

(12) Pasinetti, G. M. Cyclooxygenase and inflammation in Alzheimer's disease: experimental approaches and clinical interventions. *J. Neurosci. Res.* **1998**, *54*, 1−6.

(13) Taketo, M. M. Cyclooxygenase-2 inhibitors in tumorigenesis (part I). *J. Natl. Cancer Inst.* **1998**, *90* (20), 1529−1536.

(14) Wallace, J. L. Distribution and expression of cyclooxygenase (COX) isoenzymes, their physiological roles, and the categorization of nonsteroidal antiinflammatory drugs (NSAIDs). *Am. J. Med.* **1999**, *13*, 11s−16s.

(15) Penning, T. D.; Talley, J. J.; Bertenshaw, S. R.; Carter, J. S.; Collins, P. W.; Docter, S.; Graneto, M. J.; Lee, L. F.; Malecha, J. W.; Miyashiro, J. M.; Rogers, R. S.; Rogier, D. J.; Yu, S. S.; Anderson, G. D.; Burton, E. G.; Cogburn, J. N.; Gregory, S. A.; Koboldt, C. M.; Perkins, W. E.; Seibert, K.; Veenhuizen, A. W.; Zhang, Y. Y.; Isakson, P. C. Synthesis and biological evaluation of the 1,5-Diarylpyrazole class of cyclooxygenase-2 inhibitors: identification of 4-[5-(4-methylphenyl)-3-(trifluoromethyl)-1H-pyrazol-1-yl]benzenesulfonamide (SC-58635, Celecoxib). *J. Med. Chem.* **1997**, *40*, 1347−1365.

(16) Kurumbail, R. G.; Stevens, A. M.; Gierse, J. K.; McDonald, J. J.; Stegeman, R. A.; Pak, J. Y.; Gildehaus, D.; Miyashiro, J. M.; Penning, T. D.; Seibert, K.; Isakson, P. C.; Stallings, W. C. Structural basis for selective inhibition of cyclooxygenase-2 by antiinflammatory agents. *Nature* **1996**, *384* (19), 644−648.

(17) Picot, D.; Loll, P. J.; Garavito, R. M. The X-ray crystal structure of the membrane protein prostaglandin H2 synthase-1. *Nature* **1994**, *367*, 243−247.

(18) Marnett, L. J.; Kalgutkar, A. S. Design of selective inhibitors of cyclooxygenase-2 as nonulcerogenic antiinflammatory agents. *Curr. Opin. Chem. Biol.* **1998**, *2*, 482−490.

(19) Gierse, J. K.; McDonald, J. J.; Hauser, S. D.; Rangwala, S. H.; Koboldt, C. M.; Seibert, K. A single amino acid difference between cyclooxygenase-1 (COX-1) and −2 (COX-2) reverse the selectivity of COX-2 specific inhibitors. *J. Biol. Chem.* **1996**, *271*, 15810−15814.

(20) Plount Price, M. L.; Jorgensen, W. L. Analysis of binding affinities for celecoxib analogues with COX-1 and COX-2 from combined Docking and Monte Carlo simulations and insight into the COX-2/COX-1 selectivity. *J. Am. Chem. Soc.* **2000**, *122*, 9455−9466.

(21) Wesolowski, S. S.; Jorgensen, W. L. Estimation of binding affinities for Celecoxib analogues with cox-2 via Monte Carlo-extended liner response. *Bioorg. Med. Chem. Lett.* **2002**, *12*, 267−270.

(22) Chavatte, P.; Yous, S.; Marot, C.; Baurin, N.; Lesieur, D. Three-dimensional quantitative structure−activity relationships of cyclooxygenase-2 (COX-2) inhibitors: a comparative molecular field analysis. *J. Med. Chem.* **2001**, *44*, 3223−3230.

(23) Wang, L.; Duan, Y.; Stouten, P.; De Lucca, G. V.; Klabe, R. M.; Kollman, P. Does a diol cyclic urea inhibitor of HIV-1 protease bind tighter than its corresponding alcohol form? A study by free energy perturbation and continuum electrostatics calculations. *J. Comput.-Aided Mol. Des.* **2001**, *15* (2), 145−156.

(24) Morris, G. M.; Goodsell, D. S.; Huey, R.; Hart, W. E.; Halliday, S.; Belew, R.; Olson, A. J. *Autodock Version 3.0.3*. The Scripps Research Institute, Molecular Graphics Laboratory, Department of Molecular Biology: 1999.

(25) Morris, G. M.; Goodsell, D. S.; Halliday, R. S.; Huey, R.; Hart, W. E.; Belew, R. K.; Olson, A. J. Automated docking using Lamarckian genetic algorithm and empirical binding free energy function. *J. Comput. Chem.* **1998**, *19*, 1639−1662.

(26) Huang, X.; Xu, L.; Luo, X.; Fan, K.; Ji, R.; Pei, G.; Chen, K.; Jiang, H. Elucidating the inhibiting mode of AHPBA derivatives against HIV-1 protease and building predictive 3D-QSAR models. *J. Med. Chem.* **2002**, *45* (2), 333−343.

(27) Broughton, H. B. A method for including protein flexibility in protein−ligand docking: improving tools for database mining and virtual screening. *J. Mol. Graphics Modell.* **2000**, *18*, 2457−257.

(28) Cramer, M.; Cramer, R. D., III; Jones, D. M. Comparative molecular field analysis. 1. Effect of shape on binding of steroids to carrier proteins. *J. Am. Chem. Soc.* **1988**, *110*, 5959−5967.

(29) Klebe, G.; Abraham, U.; Mietzner, T. Molecular similarity indices in a comparative analysis (CoMSIA) of drug molecules to correlate and predict their biological activity. *J. Med. Chem.* **1994**, *37*, 4130−4146.

(30) *Sybyl, Version 6.7*. Tripos Associates: St. Louis, MO, 2000.

(31) Purcel, W. P.; Singer, J. A. *J. Chem. Eng. Data* **1967**, *12*, 235−246. Details of the implementation are given in *Sybyl 6.5 Theory Manual*; Tripos: St. Louis, MO, 1998; p 69.

(32) Morris, G. M.; Goodsell, D. S.; Huey, R.; Olson, A. J. Distributed automated docking of flexible ligands to proteins: parallel applications of AutoDock 2.4. *J. Comput.-Aided Mol. Des.* **1996**, *10*, 293−304.

(33) Solis, F. J.; Wets, R. J. B. Minimization by random search techniques. *Maths Opera. Res.* **1981**, *6*, 19−30.

(34) Weiner, S. J.; Kollman, P. A.; Case, D. A.; Singh, C.; Ghio, G.; Alagona, S.; Profeta, P.; Weiner, P. *J. Am. Chem. Soc.* **1984**, *106*, 765−784. Details of the implementation are given in *Sybyl 6.5 Theory Manual*; Tripos: St. Louis, MO, 1998; p 441.

(35) Ghose, A. K.; Viswanadhan, V. N.; Wendoloski, J. J. A knowledge-based approach in designing combinatorial or medicinal chemistry libraries for drug discovery. 1. A qualitative and quantitative characterization of known drug databases. *J. Comb. Chem.* **1999**, *1*, 55−68.

(36) POV-ray-Team. *POV-ray, version 3*; 1999 (www.povray.org).

(37) *Microcal Original Version 6.0*; 1999 (www.microcal.com).

(38) Wallace, A. C.; Laskowski, R. A.; Thornton, J. M. LIGPLOT: A program to generate schematic diagrams of protein−ligand interactions. *Protein Eng.* **1995**, *8*, 127−134.

(39) Gierse, J. K.; MeDonald, J. J.; Hauser, S. D.; Rangwala, S. H.; Koboldt, C. M.; Seibert, K. A Single Amino Acid Difference between Cyclooxygenase-1 (COX-1) and -2(COX-2) Reverses the Selectivity of COX-2 Specific Inhibitors. *J. Biol. Chem.* **1996**, *271*, 15810−15814.

(40) Wong, E.; Bayly, C.; Waterman, H. L.; Riendeau, D.; Mancini, J. A. Conversion of Prostaglandin G/H Synthase-1 into an Enzyme Sensitive to PGHS-2-selective Inhibitors by a Double His[513]→Arg and Ile[523]→Val Mutation. *J. Biol. Chem.* **1997**, *272*, 9280−9286.

(41) Stahle, L.; Wold, S. Multivariate data analysis and experimental design in biomedical research. *Prog. Med. Chem.* **1988**, *25*, 291−338.

(42) Bhattacharyya, D. K.; Lecomte, M.; Rieke, C. J.; Garavito, M.; Smith, W. L. Involvement of Arginine120, Glutamate524, and Tyrosine355 in the Binding of Arachidonate and 2-Phenyl-propionic Acid Inhibitors to the Cyclooxygenase Active Site of Ovine Prostaglandin Endoperoxide H Synthase-1. *J. Biol. Chem.* **1996**, *271*, 2179−2184.